

Microwave emission by nonlinear crystals irradiated with a high-intensity, mode-locked laser

A F Borghesani¹, C Braggio² and M Guarise²

¹CNISM Unit, Department of Physics and Astronomy, University of Padua
and Istituto Nazionale di Fisica Nucleare, Sez. Padova
Via F. Marzolo 8, I-35131 Padua, Italy

²Department of Physics and Astronomy, University of Padua
and Istituto Nazionale di Fisica Nucleare, Sez. Padova
Via F. Marzolo 8, I-35131 Padua, Italy

E-mail: armandofrancesco.borghesani@unipd.it

Abstract. We report on the experimental investigation of the efficiency of some nonlinear crystals to generate microwave (RF) radiation as a result of optical rectification (OR) when irradiated with intense pulse trains delivered by a mode-locked laser at 1064 nm. We have investigated lithium triborate (LBO), lithium niobate (LiNbO₃), zinc selenide (ZnSe), and also potassium titanyl orthophosphate (KTP) for comparison with previous measurements. The results are in good agreement with the theoretical predictions based on the form of the second-order nonlinear susceptibility tensor. For some crystals we investigated also the second harmonic generation (SHG) to cross check the theoretical model. We confirm the theoretical prediction that OR leads to the production of higher order RF harmonics that are overtones of the laser repetition rate.

PACS numbers: 42.70.Mp, 42.65.-k, 42.65.Ky

Keywords: nonlinear crystals, optical rectification, microwaves, mode-locked lasers, second harmonic generation

Submitted to: *J. Opt.*

1. Introduction

Nonlinear Optics is a well established branch of Physics [1, 2]. The discovery of materials with nonlinear optical properties has paved the way to the vast realm of optical frequency conversion. Among the most important applications there is second harmonic generation (SHG). Also optical rectification (OR) in nonlinear electro-optic crystals is a well known phenomenon [3–5] that has been exploited for the production of (sub)picosecond, microwave and terahertz bandwidth radiation as a consequence of frequency mixing [6–9].

Microwave (RF) pulses are produced by several techniques based on optical heterodyning [10–12]. The beating between two nearby laser lines or between the various Fourier components of the optical spectrum of an ultrashort laser pulse produces optically rectified electrical pulses at the difference frequency in the microwave- and far infrared range (from GHz up to THz) [13–16].

In a recent Letter [17], we have reported on a different way to produce long microwave pulses by irradiating a second-order nonlinear KTiOPO_4 (KTP) crystal with 500 ns-long pulse trains delivered by a high-intensity, mode-locked laser in the near infrared at 1064 nm. The 10 ps-long pulses are repeated at a rate $f_0 \approx 4.6$ GHz. As a result, the laser spectrum is quite pure and optical rectification is obtained by only exploiting the high strength of the laser electric field.

The fast electronic, second-order response of the nonlinear crystal gives origin to a time-dependent polarization $P(t)$ that closely follows the envelope $|E_0(t)|^2$ of the intense laser pulses electric field $E(t) = E_0(t) \cos \omega_L t$, with $\omega_L = 2\pi f_L$ where f_L is the laser frequency [18]. The low-frequency branch of the Fourier spectrum of $P(t)$ contains the fundamental RF harmonic at frequency f_0 and several of its overtones. The fundamental harmonic can be easily detected by placing the crystal in a microwave cavity that acts as a narrow bandpass filter. Its amplitude dependence on the crystal orientation with respect to the laser beam polarization gives pieces of information on the crystallographic structure of the sample. This kind of technique can also be used as an inline tool to monitor the stability of a high repetition rate, mode-locked laser. The possible advantages of such a technique have recently been highlighted [19].

The technique reported in the previous Letter could be also exploited to measure the elements of the nonlinear second-order optical tensor of a given crystal in addition to the Maker-fringe technique [20] and it additionally gives the researchers the opportunity to produce microwave overtones in a controlled way.

In order to test these statements, we have carried out additional measurements of RF generation in several crystals, **which were never investigated before to this purpose**, whose crystallographic properties differ from those of KTP, and in KTP itself for comparison sake. We have chosen lithium triborate (LiB_3O_5 or, simply, LBO), lithium niobate (LiNbO_3), and zinc selenide (ZnSe) because the elements of their second-order nonlinear optic tensor are relatively well known. The measurements have been carried out by placing the crystals either in a microwave cavity or in a waveguide of much

wider passband in order to measure the microwave overtones. As RF generation is a second-order nonlinear phenomenon intimately related to optical SHG, optical second harmonic (SH) light has simultaneously been measured as a cross check of the validity of our approach.

The paper is organized as follows. In Sect. 2 the details of the experimental setup are given. In Sect. 3 the theoretical basis for the understanding of the phenomenon is described. The results are presented and discussed in Sect. 4. Finally, the conclusions are drawn in Sect. 5.

2. Experimental Setup

The experimental setup and technique have thoroughly been described elsewhere. We briefly recall here the main characteristics of the apparatus while referring to literature for details [17, 19, 21].

A home-made, infrared ($\lambda = 1046$ nm), mode-locked laser of high intensity delivers a 500 ns-long train of $N \approx 2300$, 10 ps-long pulses [22]. The repetition rate $f_0 \approx 4.6$ GHz used in our experiment is not a limiting factor as the fast electronic response of the crystals makes them responsive to lasers of much higher repetition rate [23,24]. The laser beam is linearly polarized along the \hat{y} direction and propagates along the \hat{z} direction. A half-wave plate mounted on a rotary goniometer in the beam path can be rotated through an angle θ to rotate the beam polarization through an angle 2θ with respect to the original direction. Then, the beam impinges onto the entrance face of the crystal. The laser beam has an ellipsoidal Gaussian profile with effective area $S \approx 2.6$ mm² **and its intensity averaged over the spot size is I** . It can be reduced by inserting calibrated neutral density filters in beam path and is measured with a bolometer (Coherent, mod. J-25-MB-IR).

The crystals under investigation, of typical size $4 \times 4 \times 10$ mm³, are cut in the shape of a right square prism with the long edge directed along the \hat{z} direction and the square face lying in the (\hat{x}, \hat{y}) plane. In order to investigate the fundamental RF harmonic, the crystal is placed in a rectangular RF cavity designed so as to sustain a TE₁₀₁ mode tuned to the laser repetition rate. If higher RF harmonics are to be detected, the crystal is placed in a coaxial waveguide consisting of two concentric cylindrical conductors of inner and outer diameter 3.9 mm and 9.1 mm, respectively, that is designed to support TEM modes up to ≈ 12 GHz and TE and TM modes of higher frequency [21, 25].

When the cavity is used, the crystal is mounted on a rotary goniometer and can be rotated through an angle θ_c in order to maximize the RF signal detected by a critically coupled antenna. The electrical power transferred to the cavity field is $\propto |\mathbf{E}_{\text{RF}} \cdot \mathbf{j}|$, where \mathbf{j} is the polarization current density [26]. Thus, we expect that RF signal shows two maxima and two minima for a complete turn of the axis about its \hat{z} axis as is shown in Figure 1, in which we plot how the RF signal amplitude V_{RF} of the KTP crystal and the resonance frequency f_0 of the cavity vary with the crystal alignment with respect to the cavity mode polarization. Similar results are obtained with all other crystals. We note

that a crystal rotation about one of its geometrical symmetry axis can only maximally align the polarization along the cavity mode polarization because the geometrical axes may not coincide with the crystallographic ones. **We believe that this misalignment is responsible for the asymmetry of V_{RF} as a function of the angle θ_c .** We further note that f_0 is the lowest when V_{RF} is the largest.

The light exiting the opposing crystal face contains both contributions of the pump laser and of the second harmonic (SH) and exits the cavity through a small opening. The infrared component is filtered out by means of a suitable combination of harmonics separators and bandpass filters so that the SH component can be measured by a photodiode. When the waveguide is used, no provisions are made to optimize the crystal orientation and to measure the SH.

The RF signal amplitude is so large that it can directly be observed with the oscilloscope (LeCroy, mod. WaveRunner 6000A for the cavity- and LeCroy, mod. LabMaster/SDA/DDA 8Zi-B for the waveguide measurements), except for the LBO crystal, for which we used a 38 dB-gain microwave amplifier (Miteq, mod. AMF-4D-001120220-10P).

The amplitude of the RF emission is obtained by fitting a Lorentzian function to the numeric Fourier transform of the recorded RF signal. The conversion factor between the Lorentzian amplitude and the actual rms RF amplitude is simply $1/\sqrt{M/4\pi}$, where M is the number of points sampled by the oscilloscope.

3. Theoretical background

The observed phenomenon is explained by introducing the crystal second-order nonlinear optical susceptibility tensor of elements d_{ijk} . The laser electric field after the half-wave plate at the crystal entrance face can be written as

$$\mathbf{E}(t) = E_0 \hat{\mathbf{e}} \cos(\omega_L t) u(t, \Delta, \tau, N) \quad (1)$$

in which E_0 is its amplitude and $\hat{\mathbf{e}}$ is its polarization vector given by

$$\hat{\mathbf{e}} = \begin{pmatrix} \cos 2\theta \\ \sin 2\theta \\ 0 \end{pmatrix} \quad (2)$$

The function u represents the pulse train and can be written as

$$u(t, \Delta, \tau, N) = \sum_{m=0}^{N-1} [H(t - m\Delta) - H(t - m\Delta - \tau)] \quad (3)$$

in which the pulses are assumed rectangular. H is the Heaviside step function, $\Delta = f_0^{-1}$ is the time interval between pulses, $\tau \approx 10$ ps is the pulse duration, and N is the number of pulses in the train. f_0 is the pulses repetition rate and, thus, the fundamental RF harmonic. Actually, the pulses have a sech^2 shape but this fact does not affect the conclusions we draw.

Limiting our attention to second-order phenomena, the cartesian components of the nonlinear polarization produced by the strong laser field are

$$P_i = 2 \sum_{jk} d_{ijk} E_j E_k \quad (4)$$

By introducing the time dependence of the field, we get for the polarization

$$\begin{aligned} P_i(t) &= E_0^2 [1 + \cos(2\omega_L t)] u(t, \Delta, \tau, N) \sum_{jk} d_{ijk} \hat{e}_j \hat{e}_k \\ &= P_i^{\text{OR}} + P_i^{\text{SHG}} \end{aligned} \quad (5)$$

The first term in square brackets gives the OR contribution whereas the second one is responsible for the SHG. The structure of the quasistatic polarization due to OR is

$$P_i^{\text{OR}}(t) = E_0^2 u(t, \Delta, \tau, N) \sum_{jk} d_{ijk} \hat{e}_j \hat{e}_k \quad (6)$$

The factor E_0^2 is proportional to the laser intensity I . Owing to the presence of the function $u(t, \Delta, \tau, N)$, the Fourier spectrum of P_i^{OR} is a comb of regularly spaced frequencies that are integer multiples of the fundamental harmonic f_0 [27]. In our experiment, $4.6 \text{ GHz} \leq f_0 \leq 4.7 \text{ GHz}$ and the spectrum extends roughly up to a frequency $f_M = \tau^{-1} \approx 100 \text{ GHz}$. Finally, the sum involving the elements of the second-order nonlinear optical susceptibility tensor and the components of the vector \hat{e} must in general be a function h_i of the rotation angle θ of the half-wave plate of the form

$$h_i \equiv h_i(4\theta, d_{ijk}) = \sum_{jk} d_{ijk} \hat{e}_j \hat{e}_k \quad (7)$$

The 4-fold periodicity stems from the quadratic terms $\hat{e}_j \hat{e}_k$. The actual analytic form of h_i depends on the crystals via the explicit form of d_{ijk} but it is time independent and does not modify the spectral composition of P_i^{OR} that can be thus expanded in Fourier series

$$P_i^{\text{OR}}(t) = I h_i(4\theta, d_{ijk}) \sum_l p_l \cos(2\pi l f_0 t) \quad (8)$$

Here, the amplitude coefficient p_l of the l -th RF harmonic depends on the Fourier transform of the actual shape of u .

It can be shown [26, 28] that, in the condition of our experiment, the amplitude of the RF field radiated by the crystal is proportional to the second time derivative of the slowly varying dielectric polarization

$$\ddot{P}_i^{\text{OR}} \propto I h_i(4\theta, d_{ijk}) f_0^2 \sum_l l^2 p_l \cos(2\pi l f_0 t) \quad (9)$$

Thus, the RF signal detected in our apparatus is proportional to it. All harmonics should be proportional to the laser intensity and share the same angular behaviour.

Similarly, the spectrum of the SH radiation emitted by the crystal, which is the time-averaged square modulus of the second time derivative of P_i^{SHG} , consists in a restricted-band frequency comb centered around the frequency $2f_L \approx 5.64 \times 10^{14} \text{ Hz}$

and width of order $\tau^{-1} \approx 100 \text{ GHz} \ll 2f_L$ so that all frequencies are in the optical region. As a result, the integrated intensity I_{SH} can be cast in the form

$$I_{\text{SH}} \propto \left\langle \left| \left(\ddot{P}_i^{\text{SHG}} \right) \right|^2 \right\rangle \propto I^2 v_i(8\theta, 4\theta, d_{ijk}) \quad (10)$$

in which

$$v_i \equiv v_i(8\theta, 4\theta, d_{ijk}) = \sum_{jklm} d_{ijk} d_{ilm} \hat{e}_j \hat{e}_k \hat{e}_l \hat{e}_m \quad (11)$$

The 8- and 4-fold periodicity stems from the quartic terms in \hat{e} .

We note that the elements of the nonlinear second-order susceptibility tensor for OR, d_{ijk}^0 , and for SHG, $d_{ijk}^{2\omega_L}$, could in principle be different but we have shown that in this experiment they actually are equal so that no superscript is needed to tag them [17].

Finally, as a consequence of the symmetry with respect to the interchange of indices j and k in (4), we will use the contracted indices form of the optical tensor that is represented by a 3×6 matrix of elements d_{il} that operates on the E^2 column vector to yield the amplitude of the second-order nonlinear polarization [1].

4. Experimental Results and Discussion

In this section we present and discuss the results obtained about the efficiency and properties of the microwave produced by several nonlinear crystals in both microwave cavity and waveguide. We anticipate that the results obtained with the two different experimental setups are consistent with each other.

4.1. Materials

We have investigated the following crystals: LBO, LiNbO₃, ZnSe, and KTP. **As this experiment is not aimed at SHG, the crystals are not specifically cut to obtain phase matching.** Their crystallographic properties are summarized in Table 1.

Table 1. Crystallographic properties

Crystal	Structure	Group	Nonzero d_{il} elements
LBO	orthorombic	$2mm$	$d_{15}, d_{24}, d_{31}, d_{32}, d_{33}$
LiNbO ₃	trigonal	$R3c$	$d_{15}, d_{16}, d_{21}, d_{22}, d_{24}$ d_{31}, d_{32}, d_{33}
ZnSe	cubic zincblende	$\bar{4}3m$	d_{14}, d_{25}, d_{36}
KTP	orthorombic	$2mm$	$d_{15}, d_{24}, d_{31}, d_{32}, d_{33}$

For KTP, only three out of the five nonzero coefficients are independent as $d_{15} = d_{31}$ and $d_{24} = d_{32}$. Their values are $d_{15} = 1.73$, $d_{24} = 3.45$, and $d_{33} = 13.5$ [29]. The tensor elements of LBO are smaller than those of KTP and their values are $d_{15} = -0.897$, $d_{24} = 0.958$, $d_{31} = -0.854$, $d_{32} = 0.992$, and $d_{33} = 0.057$ [30]. For LiNbO₃, only three tensor elements are independent as $d_{15} = -d_{24} = d_{31} = d_{32}$, $d_{16} = d_{21} = -d_{22}$, and

$d_{32} = d_{31}$. Their values are $d_{15} = -4.3$, $d_{16} = -2.1$, and $d_{33} = -27$ [31]. All values are expressed in pm/V. Finally, ZnSe, though optically isotropic, is not endowed with an inversion center and its only three non vanishing tensor elements are equal to each other with value $d_{14} = d_{25} = d_{36} = 33$ pm/V [32, 33]. We have to note that the spread of the values reported in literature is quite large.

4.2. RF generation efficiency

According to (9), the amplitude of the signal detected by the antenna in the cavity or measured in the waveguide, V_{RF} , is proportional to the laser intensity I for a fixed direction θ of the laser beam polarization and at constant laser repetition rate f_0 .

We report in Figure 2 the linear relationship between V_{RF} and I measured for all crystals. For ZnSe we used a weaker I because of its smaller damage threshold. The observed linearity confirms that the generation of RF is a second-order nonlinear effect. We note that ZnSe is the most efficient crystal and LBO is the least efficient one. ZnSe is ≈ 3.6 times more efficient than KTP and ≈ 7 times more efficient than LiNbO₃, and, finally, ≈ 700 times more efficient than LBO. Qualitatively, this result mirrors the value of the largest tensor element of each crystals. The largest coefficient is that of ZnSe, the smallest belonging to LBO. Unfortunately, the slope of the $V_{\text{RF}} - I$ relationship is not related in a simple way to the elements d_{il} of the optical tensor so that no easy quantitative comparison is possible with a theoretical prediction [17].

In the waveguide, we have been able to detect several higher order RF harmonics, up to four for KTP and LBO and up to three for ZnSe, as shown on Figure 3. LiNbO₃ was not investigated in this experiment. The amplitude of all harmonics depends linearly on I , thereby validating (9). We note that the harmonics are not naturally ordered according to their expected strength. In KTP and ZnSe the second harmonic is stronger than the first one. Moreover, KTP appears to produce more RF than ZnSe in contrast with the cavity result. In any case, LBO is confirmed to be the least efficient. We noted that the placement of the crystal in the waveguide is a critical issue. Tiny displacements of the same crystal could lead to significant relative and absolute changes of the harmonic strengths. The reason for this behaviour might be ascribed to the strong non uniformity of the electric field distribution in the waveguide [25] that makes the positioning of the crystal hardly reproducible.

As a final remark, we note that, in the present experiment, the RF generation is not affected by the SHG because the efficiency of SHG is well below 1% [19] owing to the fact that the crystals are not cut so as to obtain phase matching at the wavelength of the experiment. Thus, the pump beam is not expected to be significantly depleted by SH conversion.

4.3. SHG efficiency

As previously mentioned, we have also carried out SHG measurements when using the microwave cavity. The SH intensity is measured with a photodiode whose output is

averaged over the duration of the laser pulse train, thus yielding V_G . All investigated crystals do actually emit light at 532 nm with different efficiency, as shown in Figure 4. As expected, according to (10), the SH intensity is a quadratic function of the laser intensity I . KTP is the less efficient of all of them whereas LiNbO₃ is the most efficient one.

4.4. RF dependence on the laser polarization

As observed in our previous experiment [17], and explained in Section 3, the microwave emission depends on the crystal axes orientation with respect to the laser polarization. This fact can be exploited to build an experimental setup for the measurement of the elements of the second-order optical tensor. To this goal, the measurements can be either carried out in a cavity or in a waveguide.

In Figure 5 we compare the amplitude of the microwave produced by KTP irradiated in the cavity with a laser intensity $I \approx 7.1 \text{ MW/cm}^2$ (open squares) and that of the 1st harmonic in the waveguide for $I \approx 9.4 \text{ MW/cm}^2$. The two sets of measurements are in good agreement.

The dependence of the RF signal on θ is due to the function $h_i(4\theta, d_{ijk})$ and, according to (9), all RF harmonics should share the same behaviour. In Figure 6 we plot the angular dependence of the first four RF harmonics of KTP measured in the waveguide at constant laser intensity $I = 9.4 \text{ MW/cm}^2$ and constant repetition rate $f_0 = 4.684 \text{ GHz}$. As expected, the angular behaviour is the same for all of them. Moreover, it is easily verified that the four curves in Figure 6 coincide if each is multiplied by a suitable constant scaling factor. The same is true also for all other crystals. Once more, this observation remarks the fact that all Fourier components of the RF spectrum share the same prefactor $Ih_i(4\theta, d_{ijk})f_0^2$.

In Figure 7 through Figure 9, we show the angular dependence of the fundamental RF harmonic amplitude measured in the cavity. For all crystals, V_{RF} shows 4-fold periodicity as a function of θ and, except ZnSe, the maximum RF production occurs at the same angle of maximum SHG. For ZnSe, the RF maximum roughly occurs at the angle at which SH is minimum and vice versa. This behaviour is related to the nonlinear tensor structure. That is why we carried out RF measurements in ZnSe for two crystal orientations θ_c that differ by 90° (Figure 9).

At constant I and f_0 , the contribution of the second-order nonlinear polarization to the amplitude of the RF signal measured in the cavity is given by the weighted sum of the contributions of each of its cartesian components

$$V_{\text{RF}} = A \sum_{i=1}^3 g_i h_i(4\theta, d_{ijk}) \quad (12)$$

in which A is a constant and g_i are the director cosines. As the relative orientation of the nonlinear polarization field relative to the cavity mode polarization is unknown, the director cosines are to be treated as adjustable parameters. However, there is less freedom than it appears because there is the strong constraint imposed by the crystal

structure via the form of the susceptibility tensor d_{ijk} that determines the analytic form of h_i given by (7), in which the components of the laser field given by (2) are expressed in the frame of reference of the crystallographic axes.

The LiNbO₃ crystal is cut along a (001) face so that the crystallographic and the geometric axes coincide. We remind that the geometrical axes are aligned to the laser polarization direction before the half-wave plate. LBO and ZnSe are cut along the (01 $\bar{1}$) face so that the polarization vector $\hat{\mathbf{e}}'$ in the crystal frame of reference is obtained by applying a rotation of amplitude $\alpha = 135^\circ$ around \hat{x}

$$\hat{\mathbf{e}}' = \begin{pmatrix} \cos 2\theta \\ \cos \alpha \sin 2\theta \\ -\sin \alpha \sin 2\theta \end{pmatrix} \quad (13)$$

The KTP crystal used in this experiment is cut at an angle $\beta \approx 165^\circ$ **because it was previously used in a different experiment to obtain phase matching at a wavelength different from the present one [34]**. In this case, the polarization vector $\hat{\mathbf{e}}'$ in the crystal frame of reference is obtained as

$$\hat{\mathbf{e}}' = \begin{pmatrix} \cos \beta \cos 2\theta \\ \sin 2\theta \\ -\sin \beta \cos 2\theta \end{pmatrix} \quad (14)$$

The solid lines in the figures are a fit to the data with a function of 4-fold periodicity whose explicit analytic is specific to each crystal. For LBO, we have

$$V_{\text{RF}} = V_0 \left\{ -\frac{\sqrt{2}}{2} d_{15} g_x \sin 4\theta + d_{24} g_y \sin^2 2\theta + g_z \left[d_{31} \cos^2 2\theta + \frac{1}{2} (d_{32} + d_{33}) \sin^2 2\theta \right] \right\} \quad (15)$$

The solid line in Figure 7 is obtained with fitting parameters: $V_0 = 0.974$ mV, $g_x = 0.0122$, $g_y = 0.835$, and $g_z = 0.550$.

For LiNbO₃ the fitting function is given by

$$V_{\text{RF}} = V_0 \left[g_x \sin 4\theta + g_y (d_{21} \cos^2 2\theta + d_{22} \sin^2 2\theta) + g_z (d_{31} \cos^2 2\theta + d_{32} \sin^2 2\theta) \right] \quad (16)$$

with values $V_0 = 4.47$ mV, $g_x = 0.561$, $g_y = 0.511$, and $g_z = -0.652$ and is shown as the solid line in Figure 8.

In the same figure, we plot the result of the analysis of the KTP crystal whose fitting function is

$$V_{\text{RF}} = V_0 \left\{ -2abg_x d_{15} \cos^2 2\theta - bg_y d_{24} \sin 4\theta + g_z \times \left(a^2 d_{31} \cos^2 2\theta + d_{32} \sin^2 2\theta + b d_{33} \cos^2 2\theta \right) \right\} \quad (17)$$

in which $a = \cos \beta$ and $b = \sin \beta$. The fitting parameters are $V_0 = 37.9$ mV, $g_x = -0.502$, $g_y = 0.580$, and $g_z = 0.641$.

Finally, in Figure 9 we show the results for ZnSe for two by 90° differing orientations of the crystal in the cavity. The ZnSe crystal is also cut along the (01 $\bar{1}$) face and the

three non vanishing tensor elements are equal to each other so that the RF amplitude has to be fitted to the function

$$V = V_0 d \left[g_x (1 + \cos 4\theta) - \sqrt{2} (g_y + g_z) \sin 4\theta \right] \quad (18)$$

in which d is the common value of the non vanishing tensor element. The solid lines in Figure 9 are obtained with $V_0 = 33.5$ mV, $g_x = 0.360$, $g_y = g_z = 0.660$ for the closed symbols and $V_0 = 39.8$ mV, $g_x = 0.965$, $g_y = 0.031$, and $g_z = 0.262$ for the open symbols. The different values of the director cosines are caused by the rotation of the crystal within the cavity. The two determinations of V_0 are compatible within the experimental accuracy.

4.5. Dependence of SH generation on the laser polarization

A byproduct of the measurements in the microwave cavity is the possibility to observe SHG. As mentioned above, V_G is a quadratic function of the laser intensity I (see Figure 4). We note that (10) predicts that the SH intensity angular dependence must be described by functions of 8θ and 4θ , only. The actual form of these functions is related to the structure of the specific crystals.

If the crystals were perfectly aligned with the detector, the radiation impinging on it would only originate from the two polarization components orthogonal to the line of sight. In the real experiment, the alignment is not perfect so that the detector response at constant I is a weighted sum of the contributions due to all cartesian components of the nonlinear polarization.

In Figure 10 we show the SH intensity as a function of θ for ZnSe (top), LBO (middle) and LiNbO₃ (bottom) measured at relatively low I . In Figure 11 we report the SH intensity measured in KTP [17] for the sake of comparison. The 8-fold periodicity is very evident in KTP whereas it is hardly observable in ZnSe for which the 4-fold periodicity is the dominant contribution. Also in LBO and LiNbO₃ the dominant contribution has a 4-fold periodicity and the 8-fold one manifests itself only as a distortion of a nearly pure sinusoidal shape of the curves.

The behaviour of the different crystals is once more related to the structure of the second-order nonlinear susceptibility tensor. The behavior of KTP has already been interpreted in our previous paper [17] and its analysis will not be repeated here.

According to (10), similarly to the RF analysis, the SH intensity can be written as the weighted sum

$$V_G(\theta) = \sum_{i=1}^3 s_i v_i(8\theta, 4\theta, d_{ijk}) \quad (19)$$

in which the analytic form of the functions v_i depend on the crystal structure and the weights s_i are adjustable coefficients.

In ZnSe the SH intensity is a nearly pure sinusoidal function of 4-fold periodicity. Its fitting function, as the crystal is cut along the (01 $\bar{1}$) face and as the three non

vanishing elements of the nonlinear tensor are equal $d_{14} = d_{25} = d_{36} \equiv d$, takes on the simple form

$$V_G = V_{G0} \left(\frac{d}{4} \right) \left\{ \left(s_x + \frac{3}{2}s_y + s_z \right) + 2s_y \cos 4\theta + \frac{1}{2} [s_y - 2(s_x + s_z)] \cos 8\theta \right\} \quad (20)$$

The solid line in Figure 10 (top) is obtained with the parameter values $V_{G0} = 9.71$ mV, $s_x = s_z = 0.250$ and $s_y = 0.935$.

For LBO, taking into account that the crystal is cut along the $(01\bar{1})$ face, the SH intensity is fitted to the function

$$V_G = V_{G0} \left\{ -\frac{1}{\sqrt{2}} d_{15} s_x \sin 4\theta + s_y d_{24} \sin^2 2\theta + s_z \left[d_{31} \cos^2 2\theta + \frac{1}{2} (d_{32} - d_{33}) \sin^2 2\theta \right] \right\} \quad (21)$$

We note that the LBO structure is such that only terms of 4-fold periodicity appear in the fitting function. The solid line in Figure 10 (middle) is obtained with fitting parameters: $V_{G0} = -77.9$ mV, $s_x = 0.609$, $s_y = 0.110$, and $s_z = -0.785$. In LiNbO_3 , the maximum SH intensity is obtained for a crystal orientation different from that at which the RF amplitude is maximum. The SH measurements are thus carried out by rotating the crystal by an angle γ around the \hat{y} axis to roughly satisfy the phase matching condition for maximum SH intensity. $V_G(\theta)$ takes the form

$$V_G = V_{G0} \left[s_x \left(-d_{15} \sin 2\gamma \cos^2 2\theta + d_{16} \cos \gamma \sin 4\theta \right)^2 + s_y \left(d_{21} \cos^2 \gamma \cos^2 2\theta - d_{24} \sin \gamma \sin 4\theta + d_{22} \sin^2 2\theta \right)^2 + s_z \left(d_{31} \cos^2 \gamma \cos^2 2\theta + d_{32} \sin^2 2\theta + d_{33} \sin^2 \gamma \cos^2 2\theta \right)^2 \right] \quad (22)$$

If γ is left as an adjustable parameter, the solid line in Figure 10 is obtained for $\gamma \approx 19^\circ$, which is very close to the value $\gamma_c \approx 14^\circ$ of the phase matching angle at $\lambda = 1064$ nm [35]. The remaining best fit parameters are $V_{G0} = 5.67$ mV, $s_x = 0.911$, $s_y = 0.412$, and $s_z = 0.024$.

Finally, the previously published [17] KTP data in Figure 11 are described by the function

$$V_G = V_{G0} \left\{ s_x (bd_{15})^2 \sin^2 4\theta + s_y (2abd_{24})^2 \sin^4 2\theta + s_z \left[d_{31}^2 \cos^4 2\theta + (a^2 d_{32})^2 \sin^4 2\theta + (d_{33}b^2)^2 \sin^4 2\theta \right] \right\} \quad (23)$$

and the solid line in the figure is obtained with parameters $V_{G0} = 374.2$ mV, $s_x = 0.162$, $s_y = -0.984$, and $s_z = 0.081$.

5. Conclusions

In this paper, we have investigated the efficiency of several second-order nonlinear crystals to generate long microwave pulses when irradiated with an intense pulse train of an infrared mode-locked laser because of optical rectification. The spectrum of the emitted microwave radiation is a comb of integer multiples of the laser repetition rate with a bandwidth determined by the single pulse length that can reach several tens of GHz. By designing a suitable receiver the desired microwave harmonic can be picked up and exploited for any given use.

We have also shown that the features of the microwaves generation depend on the crystal structure. In particular, the RF emission efficiency depends on the orientation of the crystal axes with respect to the laser polarization. We have shown that the observed angular dependence of the RF amplitude agrees well with the theoretical prediction provided that the crystal orientation with respect to the receiver can be determined. We have obtained a cross check of this achievement by measuring the SH emitted by the crystals that can be explained by the same model used for the microwaves.

This technique can in principle be exploited to measure the elements of the second-order nonlinear optical susceptibility tensor for unknown crystals provided that great attention is paid to carefully control the geometry of the experimental setup. We finally note that an inline, nearly lossless device can be designed by adopting this technique to monitor the quality of a high-repetition rate, mode-locked laser, its only frequency limitation being determined by the receiver used [19].

Acknowledgments

The authors wish to thank G. Bettella for supplying us the LiNbO₃ sample and gratefully acknowledge helpful discussions with G. Carugno and the technical assistance of E. Berto.

References

- [1] Yariv A and Yeh P 2007 *Photonics. Optical electronics in modern communications* The Oxford series in electrical and computer engineering (New York: Oxford University Press)
- [2] Bloembergen N 2007 *Nonlinear Optics Fundamentals of Photonics* ed Bahaa E A, Saleh A and Teich M C (New York: Wiley)
- [3] Franken P A, Hill A E, Peters C W and Weinreich G 1961 *Phys. Rev. Lett.* **7** 118–119 ISSN 00319007
- [4] Bass M, Franken P A, Ward J F and Weinreich G 1962 *Phys. Rev. Lett.* **9** 446–448
- [5] Bass M, Franken P A and Ward J F 1965 *Phys. Rev.* **138** A534–A542
- [6] Yang H H, Richards P L and Shen Y R 1971 *Appl. Phys. Lett.* **19** 320–323
- [7] Xu L, Zhang X and Auston D H 1992 *Appl. Phys. Lett.* **61** 1784–1786
- [8] Zhang X C, Jin Y and Ma F 1992 *Appl. Phys. Lett.* **61** 2764–2766
- [9] Rice A, Jin Y, Ma F, Zhang X C, Bliss D, Larkin J and Alexander M 1994 *Appl. Phys. Lett.* **64** 1324–1326
- [10] Bridges T J and Strnad A R 1972 *Appl. Phys. Lett.* **20** 382–384

- [11] Yao J 2009 *J. Lightwave Technol.* **27** 314–335
- [12] Khan M H, Shen H, Xuan Y, Zhao L, Xiao S, Leaird D E, Weiner A M and Qi M 2010 *Nat. Photon.* **4** 117–122
- [13] Niebuhr K E 1963 *Appl. Phys. Lett.* **2** 136–137
- [14] Lengfellner H 1987 *Opt. Lett.* **12** 184–186
- [15] Nahata A, Weling A S and Heinz T F 1996 *Appl. Phys. Lett.* **69** 2321
- [16] Nahata A and Heinz T F 1998 *Opt. Lett.* **23** 867–869
- [17] Borghesani A F, Braggio C and Carugno G 2013 *Opt. Lett.* **38** 4465–4468
- [18] Graf S, Sigg H and Bächtold W 2000 *Appl. Phys. Lett.* **76** 2647–2649
- [19] Braggio C and Borghesani A F 2014 *Rev. Sci. Instrum.* **85** 023105
- [20] Maker P D, Terhune R W, Nisenoff M and Savage M 1962 *Phys. Rev. Lett.* **8** 21–22
- [21] Borghesani A F, Braggio C, Carugno G, Della Valle F and Ruoso G 2014 Laser-induced microwave generation with nonlinear optical crystals *Proc. SPIE. Optics and its Applications VIII; Quantum Optics III* vol 9136 ed Eggleton B J, Gaeta A L, Broderick N G R, Sergienko A V, Rauschenbeutel A and Durt T pp 913609–913609–10
- [22] Agnesi A, Braggio C, Carugno G, Della Valle F, Galeazzi G, Messineo G, Pirzio F, Reali G and Ruoso G 2011 *Rev. Sci. Instrum.* **85** 115107
- [23] Krainer L, Paschotta R, Lecomte S, Moser M, Weingarten K J and Keller U 2002 *IEEE J. Quantum Electronics* **38** 1331–1338
- [24] Keller U 2003 *Nature* **424** 831–838
- [25] Pozar D M 2005 *Microwave Engineering* (New York: Wiley)
- [26] Jackson J D 1999 *Classical Electrodynamics* (New York: Wiley)
- [27] Cundiff S T and Ye J 2003 *Rev. Mod. Phys.* **75** 325–342
- [28] Griffiths D J 2013 *Introduction to Electrodynamics* (Glenview: Pearson)
- [29] Pack M V, Armstrong D J and Smith A V 2004 *Appl. Opt.* **43** 3319–3323
- [30] Lin S, Sun Z, Wu B and Chen C 1990 *J. Appl. Phys.* **67** 634–638
- [31] Roberts D A 1992 *IEEE J. Quantum Electron.* **28** 2057–2074
- [32] Kühnelt M and Wagner H P 1998 *J. Nonlinear Opt. Phys. & Mat.* **7** 553–561
- [33] Wagner H P, Kühnelt M, Langbein W and Hvam J M 1998 *Phys. Rev. B* **58** 10494–10501
- [34] Agnesi A, Pirzio F, Tomaselli A, Reali G and Braggio C 2005 *Opt. Express* **13** 5302–5307
- [35] Weis R S and Gaylord T K 1985 *Appl. Phys. A* **37** 191–203

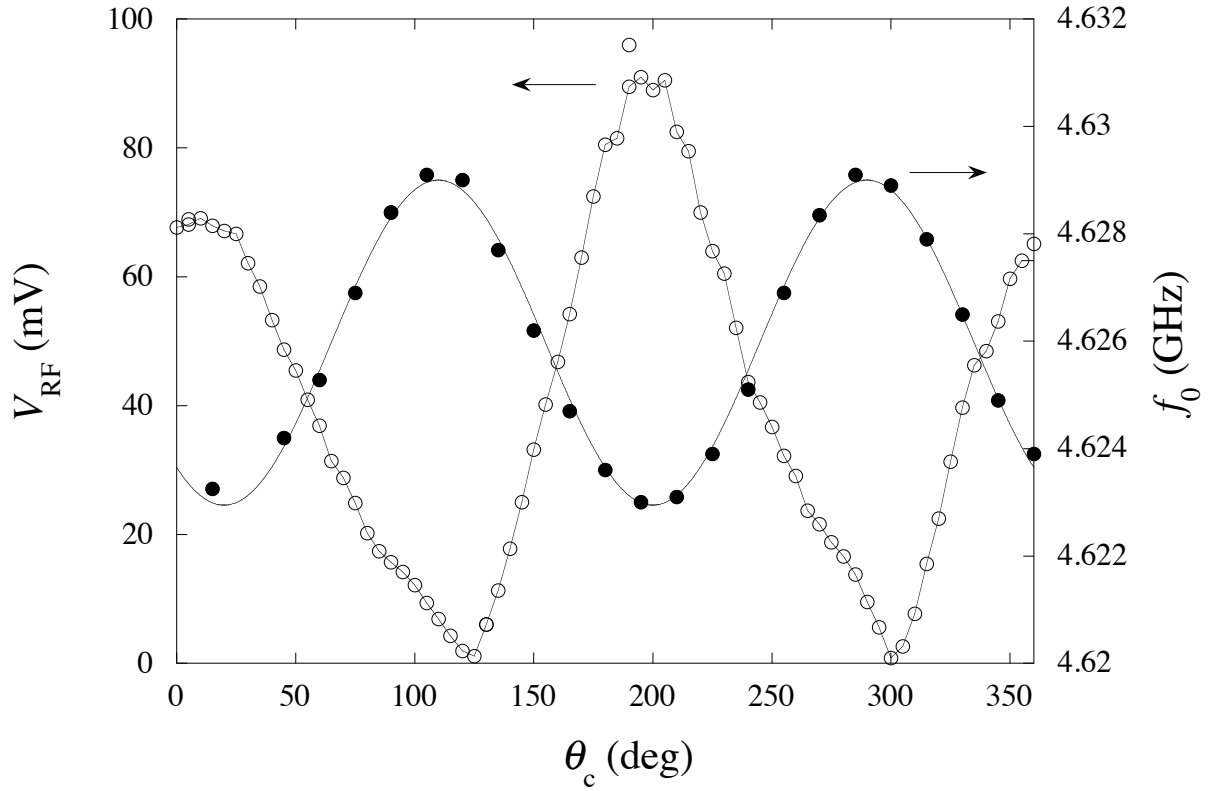


Figure 1. RF amplitude V_{RF} (open symbols, left scale) and cavity resonance frequency f_0 (closed symbols, right scale) vs θ_c for KTP. The lines are only a guide for the eyes.

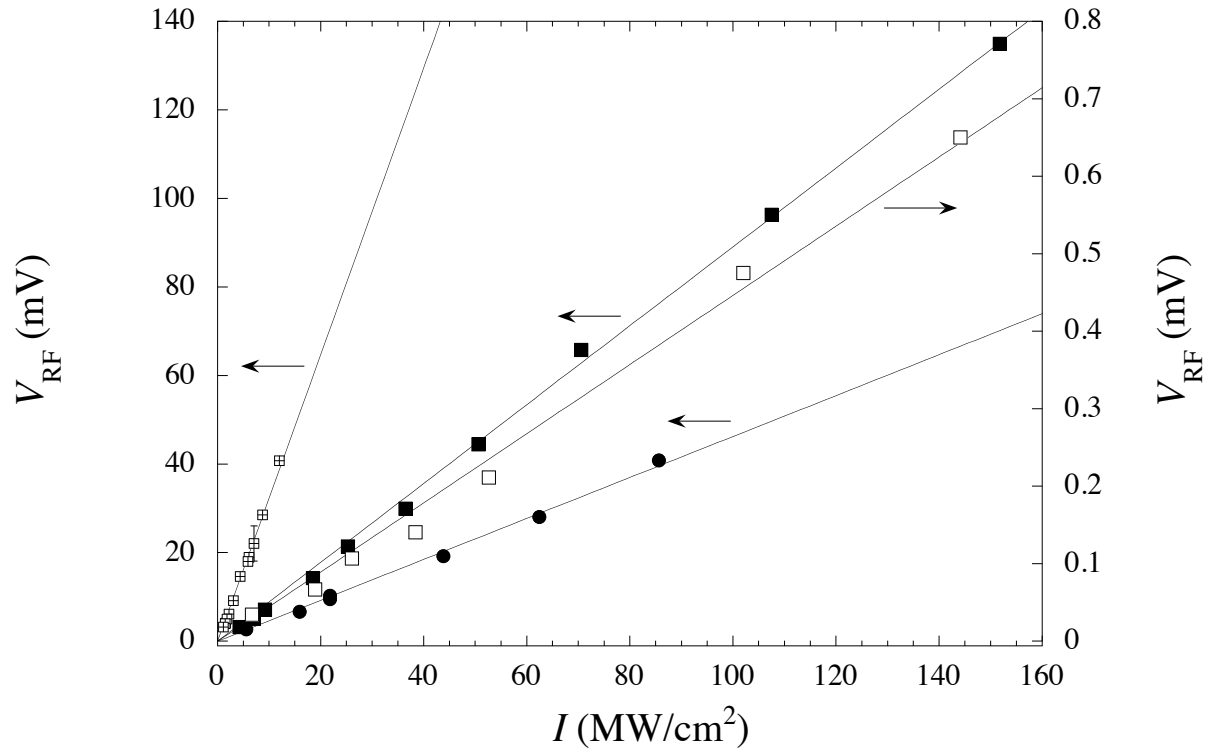


Figure 2. 1st RF harmonic amplitude V_{RF} vs I . Left scale: ZnSe (crossed squares), LiNbO₃ (closed circles), and KTP (closed squares). Right scale: LBO (open squares). The dot size is comparable to the error bars.

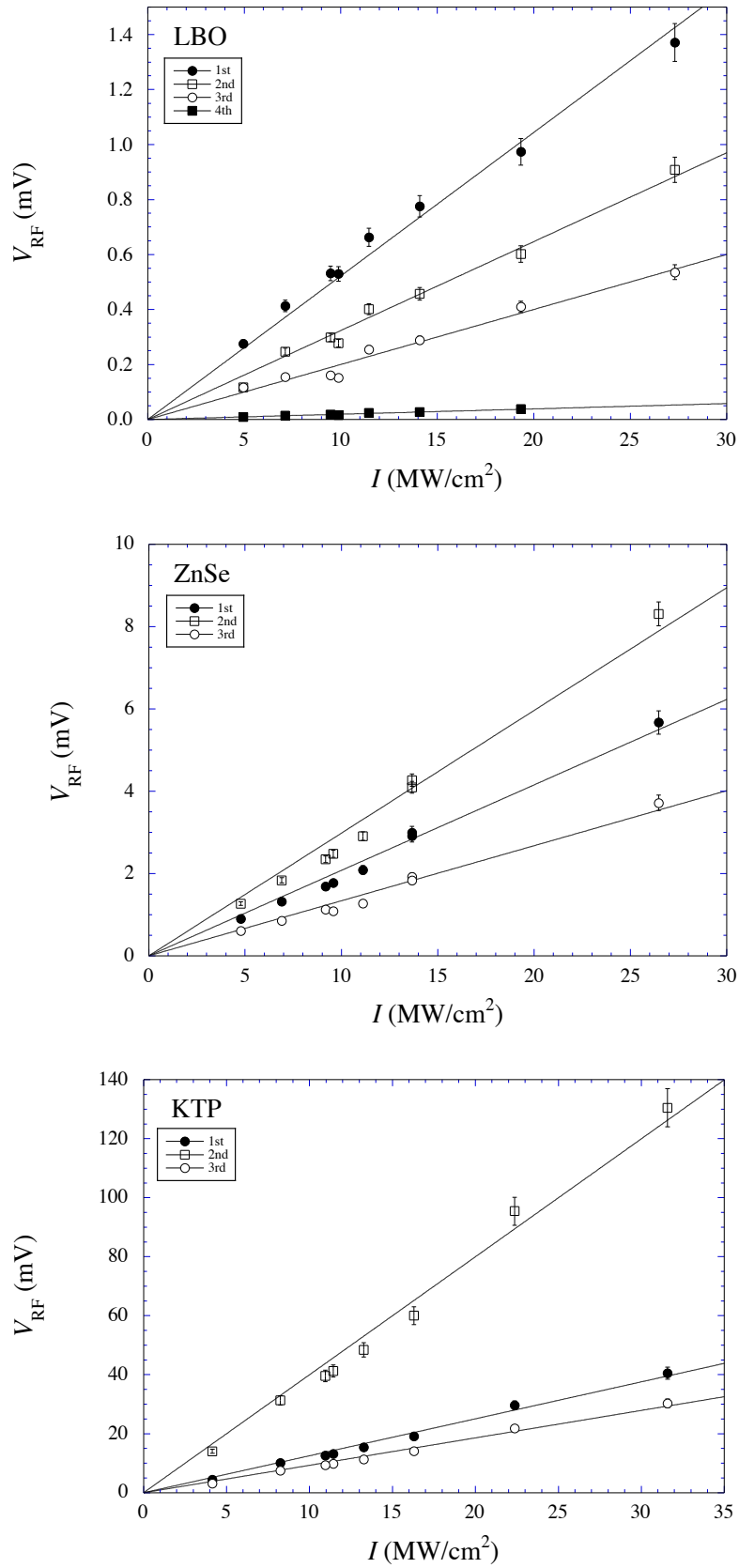


Figure 3. V_{RF} vs I for LBO, ZnSe, and KTP (from top) for the harmonics observed in the waveguide. The 4th harmonics in KTP is too small to be shown.

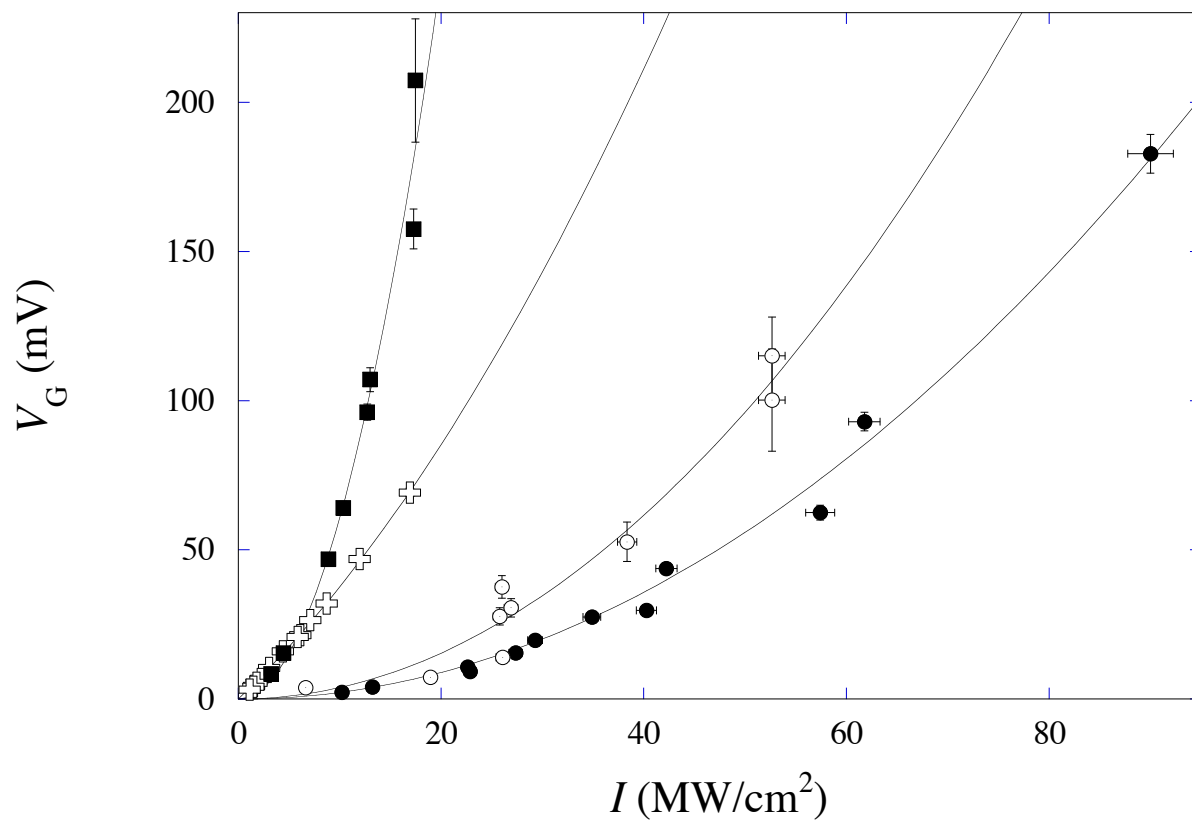


Figure 4. SH intensity V_G vs I : LiNbO₃ (squares), ZnSe (crosses), LBO (open circles), and KTP (closed circles).

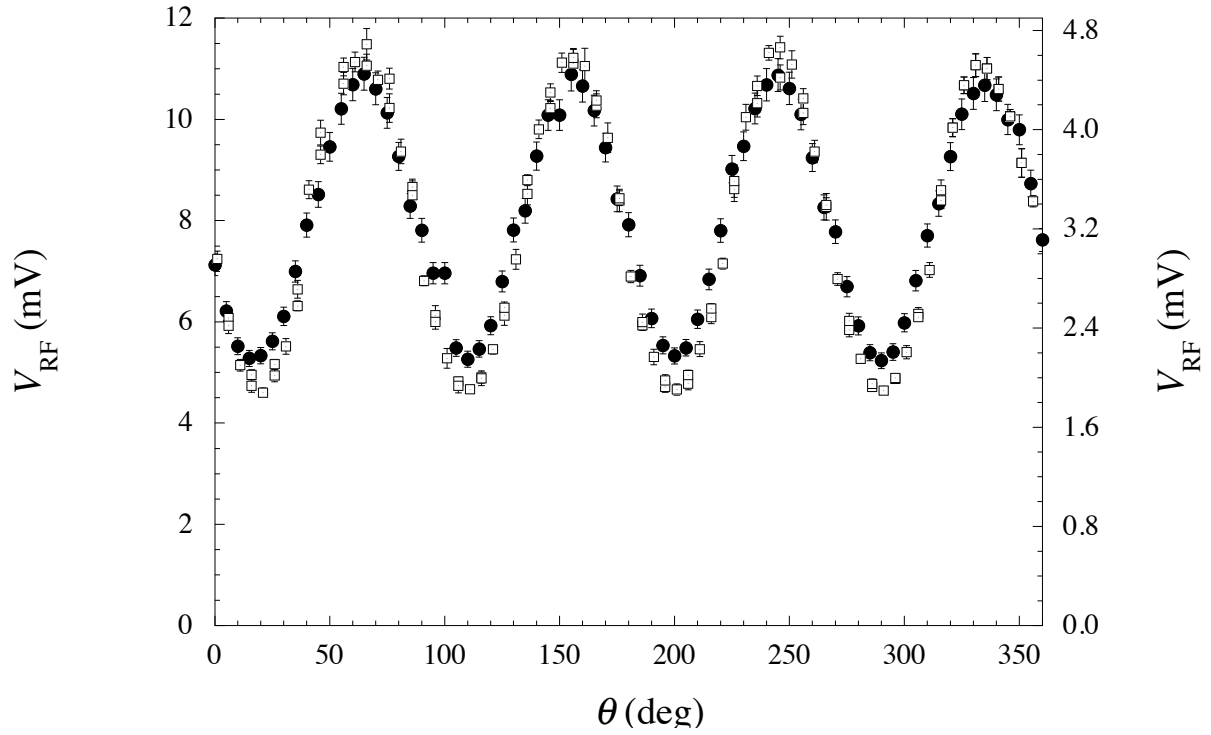


Figure 5. Comparison of the angular dependence of the RF amplitude produced by KTP in the cavity (squares, right scale) for $I = 7.1 \text{ MW/cm}^2$ and the 1st harmonic amplitude in the waveguide (circles, left scale) for $I = 9.4 \text{ MW/cm}^2$.

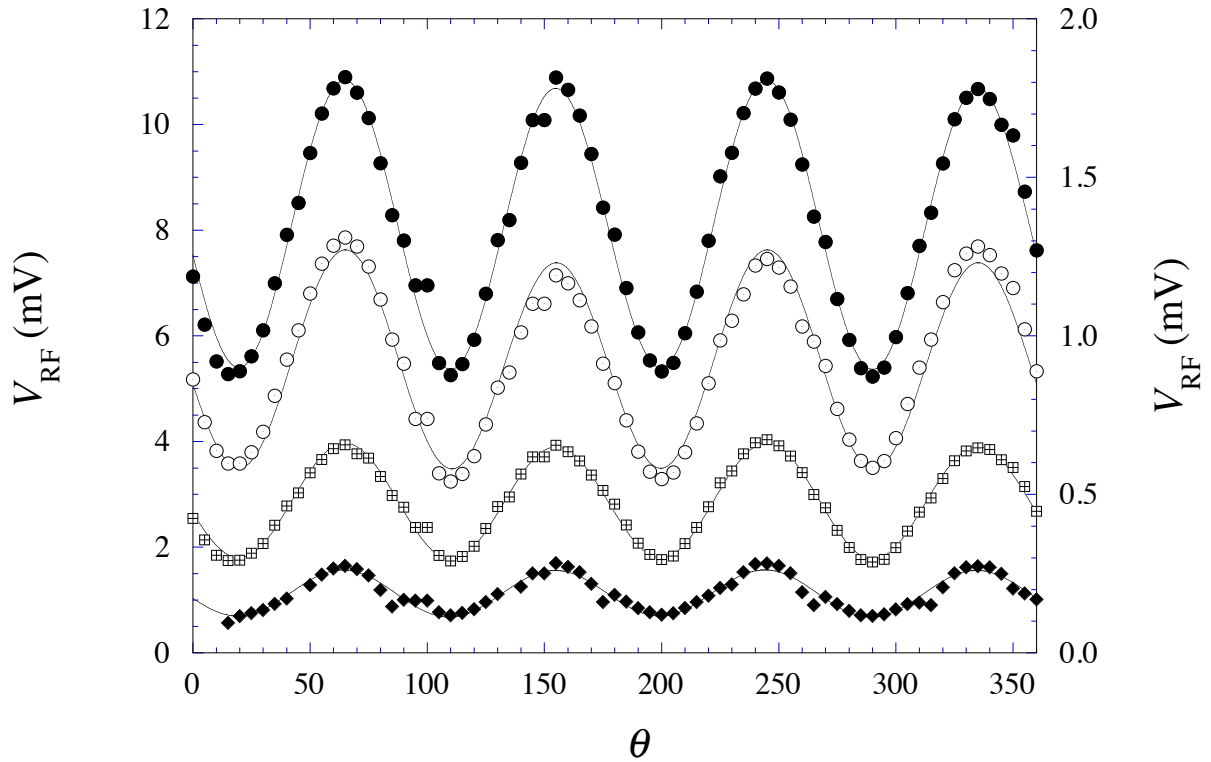


Figure 6. V_{RF} vs θ at constant $I = 9.4 \text{ MW/cm}^2$ of the first four RF harmonics produced by KTP measured using the waveguide. Left scale: 1st- (closed circle), 2nd- (open circles), and 3rd harmonic (squares). Right scale: 4th harmonic (diamonds). The lines are only eyeguides.

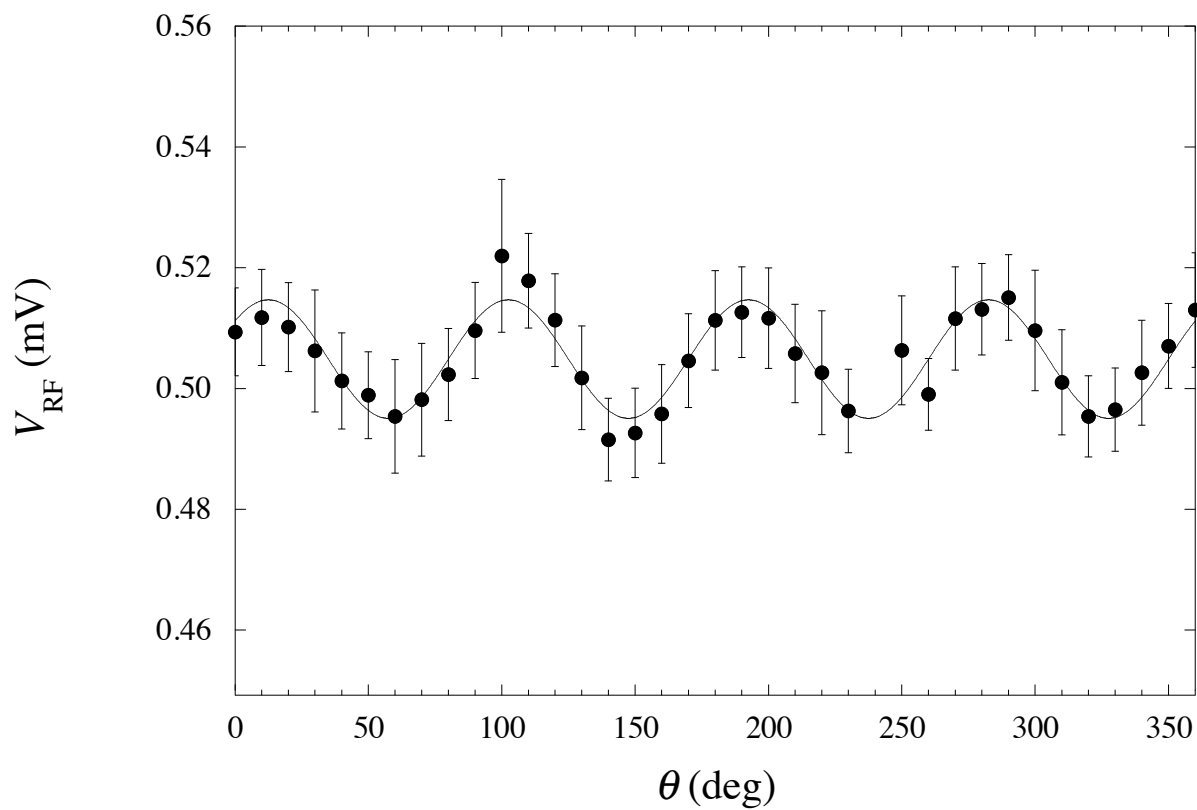


Figure 7. V_{RF} vs θ for LBO for $I \approx 96.0 \text{ MW/cm}^2$. The solid line is the model prediction.

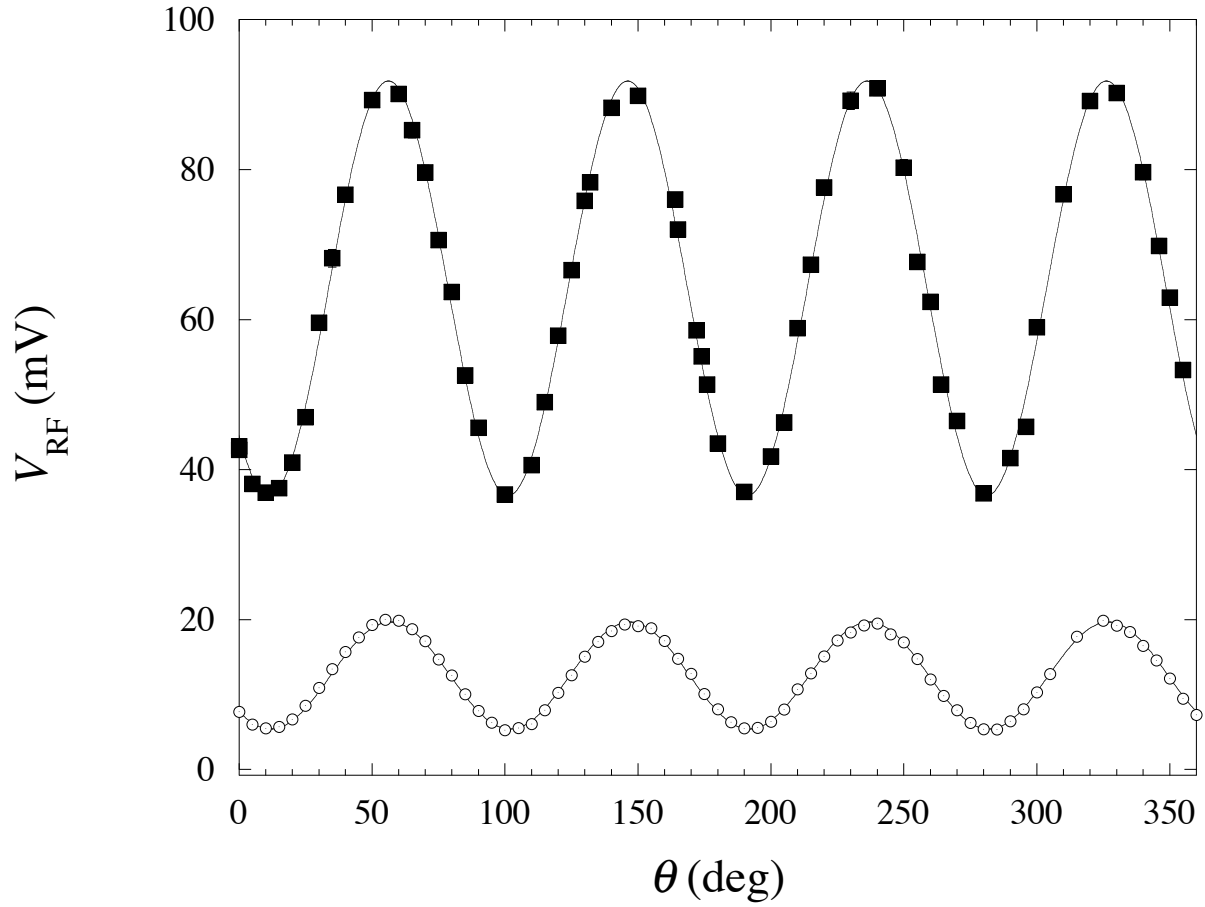


Figure 8. V_{RF} vs θ for KTP for $I \approx 107.5 \text{ MW/cm}^2$ (squares) and for LiNbO₃ (circles) for $I \approx 45.0 \text{ MW/cm}^2$. The solid lines are the model predictions. The dot size is comparable with the error bars.

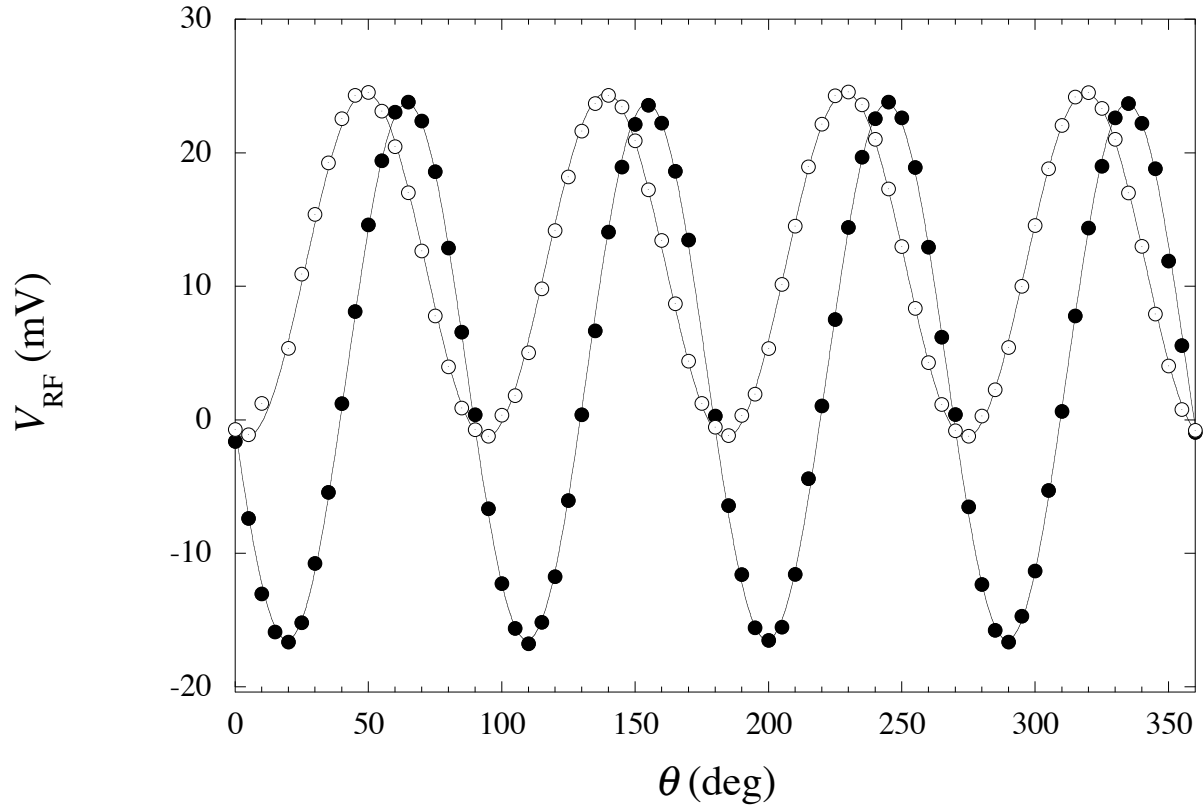


Figure 9. V_{RF} vs θ in ZnSe for $I \approx 8.1 \text{ MW/cm}^2$ for two different orientation of the crystal in the cavity. $\theta_c = 205^\circ$ (closed dots) and $\theta_c = 115^\circ$ (open dots). The lines are the model predictions. The dot size is comparable with the error bars.

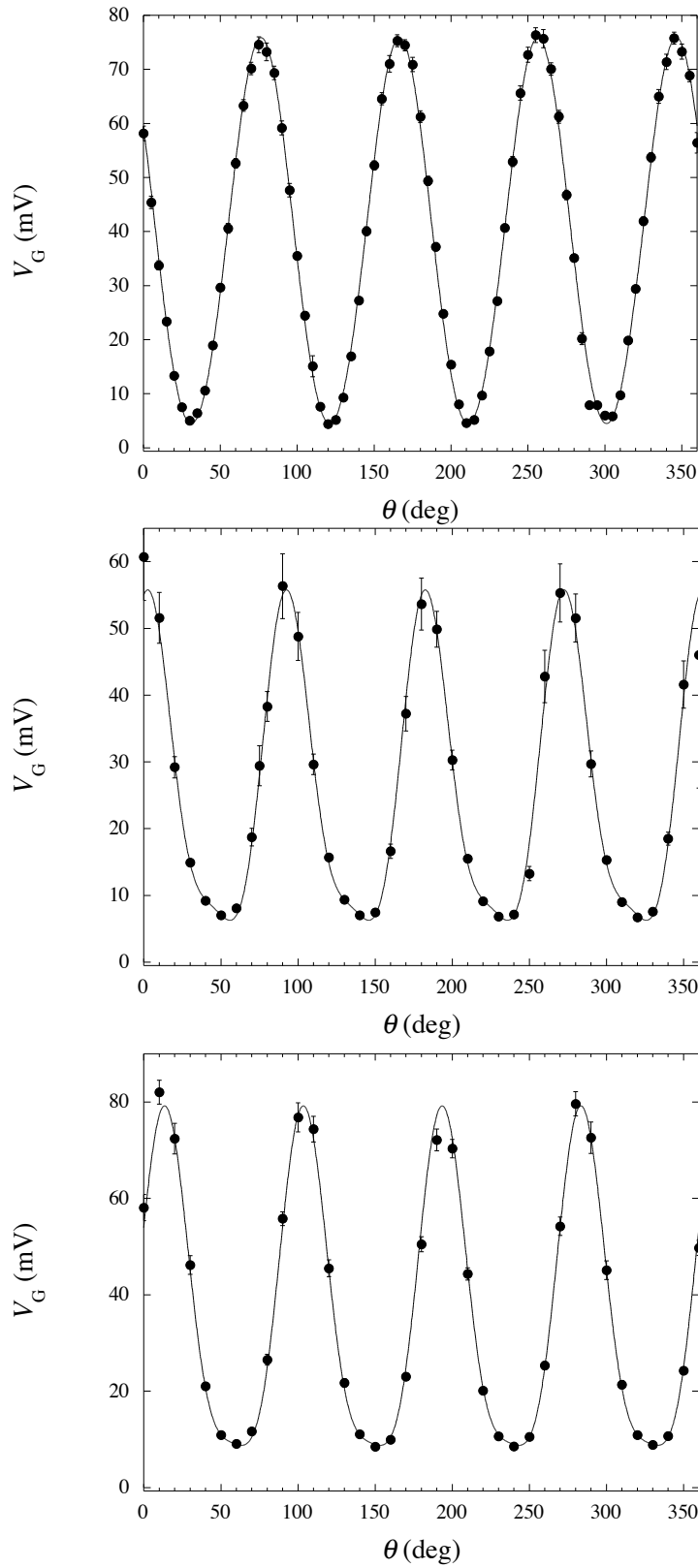


Figure 10. V_G vs θ for ZnSe (top) for $I = 18.0 \text{ MW/cm}^2$, LBO (middle) for $I = 38.4 \text{ MW/cm}^2$, and LiNbO₃ (bottom) for $I = 11.5 \text{ MW/cm}^2$. The solid lines are the predictions of the model.

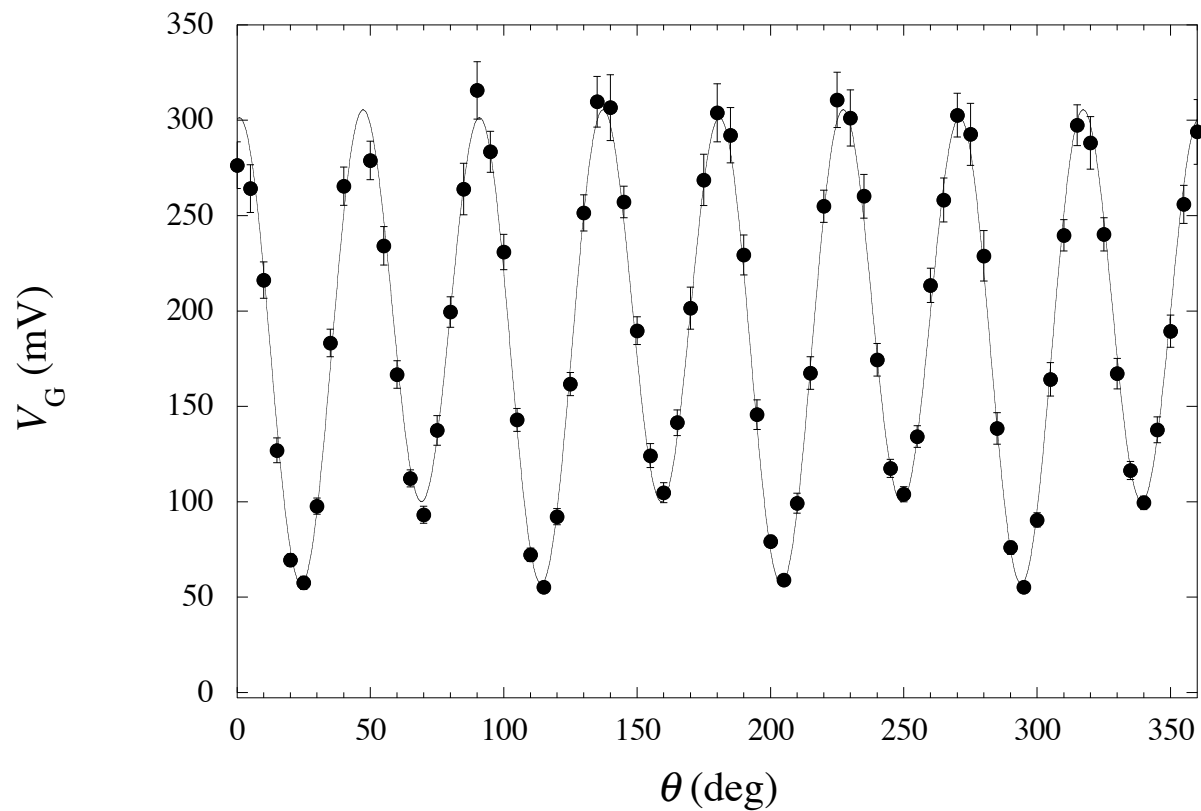


Figure 11. V_G vs θ for KTP for $I = 119.7 \text{ MW/cm}^2$ [17]. The solid lines are the predictions of the model.